Earthquakes and Structures, *Vol. 18, No. 1 (2020) 45-56*
DOI: https://doi.org/10.12989/eas.2020.18.1.045

Generation of synthetic accelerograms using a probabilistic critical excitation method based on energy constraint

Arsalan Bazrafshan[1a] and Naser Khaji *[2b]

[1] *Faculty of Civil and Environmental Engineering, Tarbiat Modares University, P.O. Box 14115–397, Tehran, Iran*
[2] *Department of Civil and Environmental Engineering, Graduate School of Engineering, Hiroshima University, 1-4-1, Kagamiyama, Higashi-Hiroshima, Hiroshima 739-8527, Japan*

(*Received January 30, 2019, Revised November 12, 2019, Accepted November 13, 2019*)

Abstract. The application of critical excitation method with displacement-based objective function for multi degree of freedom (MDOF) systems is investigated. To this end, a new critical excitation method is developed to find the critical input motion of a MDOF system as a synthetic accelerogram. The upper bound of earthquake input energy per unit mass is considered as a new constraint for the problem, and its advantages are discussed. Considering this constraint, the critical excitation method is then used to generate synthetic accelerograms for MDOF models corresponding to three shear buildings of 10, 16, and 22 stories. In order to demonstrate the reliability of generated accelerograms to estimate dynamic response of the structures, three target ground motions with considerable level of energy contents are selected to represent "real critical excitation" of each model, and the method is used to re-generate these ground motions. Afterwards, linear dynamic analyses are conducted using these accelerograms along with the generated critical excitations, to investigate the key parameters of response including maximum displacement, maximum interstory drift, and maximum absolute acceleration of stories. The results show that the generated critical excitations can make an acceptable estimate of the structural behavior compared to the target ground motions. Therefore, the method can be reliably implemented to generate critical excitation of the structure when real one is not available.

Keywords: critical excitation; non-stationary random process; total input energy per unit mass; synthetic accelerograms; energy constraint

1. Introduction

In the seismic design of structures, selection of appropriate design earthquakes is one of the most important parts of design procedure. For intermediate and low importance structures, the design earthquake is typically provided by the seismic codes as a design spectrum. However, for important structures for which time-history analysis should be performed, the use of recorded ground motions as input is inevitable. On the other hand, the available ground motions show only small part of the reality and cannot be completely trusted to predict the future events. For the design of important structures, which are expected to remain functional after earthquakes, it is highly recommended to use a worst-case analysis in order to take into account the uncertainties of the ground motions. The structural designs, which are based on critical excitation methods may greatly reduce this problem. According to critical excitation method, each structure has its own dynamic characteristics and should be designed for its critical input. This critical input is determined in such a manner that the desired quantity of the response of the structure is maximized. Critical excitation methods provide a useful tool to determine such input.

Early efforts in the field of critical excitation method were carried out by Drenick (1970), and then the method was developed to multi degree of freedom systems (Srinivasan *et al*. 1991) and nonlinear systems (Iyengar 1972). Since then, various researches have been conducted in the field of nonlinear systems (Takewaki 2002, Au 2006, Moustafa 2009, Kojima *et al*. 2018).

Instead of considering displacement as the objective function (Lekshmy and Raghukanth 2015), some researchers used other objective functions on critical excitation problems such as acceleration response (Ahmadi 1979, Takewaki 2001b), earthquake input energy (Fukumoto and Takewaki 2015), and earthquake energy input rate (Takewaki 2006). In the recent works on the critical excitation for nonlinear systems, various parameters of response such as ductility ratio, damage index, and reliability index were considered (Abbas and Manohar 2007, Moustafa 2011).

Some researchers have developed the existing methods by changing the envelope function (Ghasemi and Ashtari 2014) or the PSD function (Ashtari and Ghasemi 2013). Others tried to apply the critical excitation method in order to determine critical input for rehabilitation (Kamgar *et al*. 2015) and optimal damper design (Khatibinia *et al*. 2018, Nigdeli and Bekdas 2017, Cetin *et al*. 2019, Akehashi and Takewaki 2019). Thanks to the complexity of the problem for nonlinear systems, many researches still have focused

*Corresponding author, Professor
E-mail: nkhaji@hiroshima-u.ac.jp
[a]Ph.D. Student
[b]Ph.D.

ISSN: 2092-7614 (Print), 2092-7622 (Online)

on the linear response of the structural system (Ashtari and Ghasemi 2013, Kamgar and Rahgozar 2015, Lekshmy and Raghukanth 2015, Kamgar *et al*. 2018), while others tried to investigate nonlinear response on the simplified SDOF systems (Kojima *et al*. 2018, Tamura *et al*. 2019).

Takewaki (2001a) developed a new critical excitation method for stationary and non-stationary random input using a stochastic index of response as the objective function. Based on this method, the critical excitation is considered as rectangular spectral density function. In the present paper, the proposed Takewaki's method (2001a) is developed to determine the critical excitations for shear buildings modeled as MDOF systems. The present method does not depend on the quantity that is considered as objective function. Therefore any stochastic response index (e.g., mean square of displacement, absolute acceleration and earthquake energy input rate), which is correctly derived based on the original Takewaki's method, may be used as objective function. To the authors' knowledge, displacement-based objective functions are the most practical choice for this critical excitation method. In this paper, the sum of the mean-square interstory drift of the system is used as the objective function. The main issue of using this method is the selection of appropriate constraints. It is shown that the upper bound of earthquake input energy per unit mass may be considered as a suitable constraint for the present critical excitation problem. This bound can be a reasonable benchmark to estimate the allowable range of possible input energy in similar earthquakes. Considering this bound as the constraint, the method is used to determine the critical power spectral density (PSD) functions, as well as generation of synthetic accelerograms.

2. Critical excitation problem for MDOF systems

Consider an n-story shear building modeled as an elastic linear MDOF system with proportional damping subjected to a non-stationary random base acceleration. Input base acceleration is defined as the product of an envelope function and a stationary Gaussian random process with zero mean, as given by

$$\ddot{u}_g(t) = c(t)w(t) \tag{1}$$

The sum of the mean-square interstory drift of the shear building can be obtained from the following equation (Takewaki 2001a)

$$f = \sum_{k=1}^{n} \sigma_{D_k}(t)^2 = \int_{-\infty}^{+\infty} H(t,\omega) S_w(\omega) d\omega \tag{2}$$

where n denotes the number of stories, and $S_w(\omega)$ implies the PSD function of $w(t)$, and

$$H(t,\omega) = \sum_{k=1}^{n} \left[\left(\sum_{j=1}^{n} \Gamma_j (\phi_k^j - \phi_{k-1}^j) A_{Cj}(t,\omega) \right)^2 + \left(\sum_{j=1}^{n} \Gamma_j (\phi_k^j - \phi_{k-1}^j) A_{Sj}(t,\omega) \right)^2 \right] \tag{3}$$

in which ϕ_k^j denotes the kth component of the jth eigenvector, and Γ_j indicates the participation factor of the jth mode. In addition

$$A_{Cj}(t,\omega) = \int_0^t c(\tau) g_j(t-\tau) \cos \omega\tau d\tau \tag{4}$$

$$A_{Sj}(t,\omega) = \int_0^t c(\tau) g_j(t-\tau) \sin \omega\tau d\tau \tag{5}$$

and $g_j(t)$ is the unit impulse response function as given by

$$g_j(t) = H_e(t) \frac{1}{\omega_{dj}} e^{-h_j \omega_j t} \sin \omega_{dj} t \tag{6}$$

where ω_j and ω_{dj} represent the undamped and damped natural circular frequencies of the jth mode, h_j implies the damping ratio of the jth mode, and $H_e(t)$ is the Heaviside step function.

The critical excitation problem is now defined as follows: Given mass, stiffness and the viscous damping matrix of a linear elastic MDOF system, as well as the envelope function, find the critical PSD function $\tilde{S}_w(w)$, so that the objective function f is maximized under the following constraints

$$\int_{-\infty}^{+\infty} S_w(\omega) d\omega \le \bar{S}_w \qquad \sup S_w(\omega) \le \bar{s}_w \tag{7}$$

If the PSD function is limited, $\tilde{S}_w(w)$ can be considered as a function that has a constant value in the interval of $\tilde{\Omega} = \bar{S}_w / \bar{s}_w$, which is characterized by its limits, Ω_L and Ω_U as

$$\tilde{\Omega} = \Omega_U - \Omega_L \tag{8}$$

This input is referred as the input with rectangular PSD function. Using the rectangular PSD function, the objective function can be calculated as given by

$$f(t_i) = \bar{s}_w \int_{\Omega_L}^{\Omega_U} H(t_i, \omega) d\omega \tag{9}$$

Although adoption of a rectangular PSD for the ground shaking may seem unrealistic, there are lots of examples of recorded ground motions with a very narrow frequency content which can be properly represented by a rectangular PSD model. However, to resolve this limitation, the method can be extended by replacing the rectangular PSD by a continuous one.

To specify the location of the rectangular function (i.e., Ω_L and Ω_U) in a certain time of t_i, a horizontal line can be moved over the plot of $H(t_i, \omega)$ function so that the distance of the intersection points reaches to $\tilde{\Omega}$ as is illustrated in Fig. 1. By repeating this procedure at different time steps, the critical PSD functions are specified as rectangular functions, and the time-history of the objective function is determined. The PSD function corresponding to the maximum value of the objective function is then considered as the critical one (Takewaki 2001a).

It should be noted that the overall shape of $H(t_i, \omega)$ depends on the objective function. For some objective functions (e.g., absolute acceleration and earthquake energy input rate), $H(t_i, \omega)$ function shows a very irregular shape

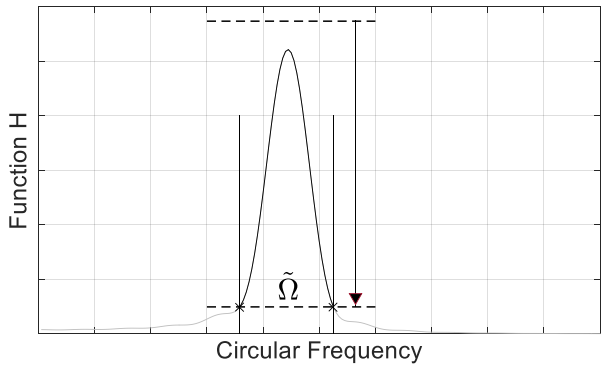

Fig. 1 Finding the critical PSD function as a rectangular function

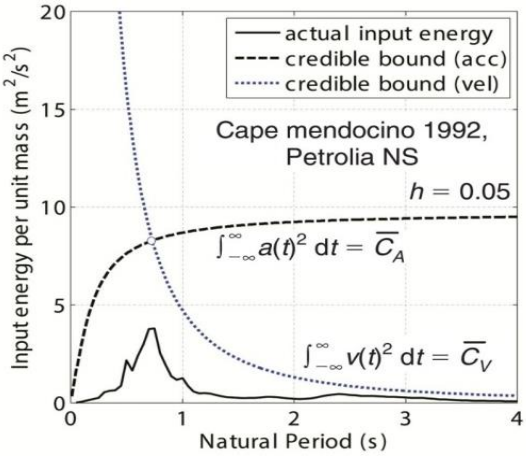

Fig. 2 Illustration of upper bounds and actual input energy of 1992 Cape Mendocino earthquake

with intense variations (see for example, Takewaki 2001b). Insuch cases, the critical PSD function may be determined as a large number of rectangles with very little widths. This situation may impose much more computational efforts to the problem. On the other hand, $H(t_i, \omega)$ function for displacement based objective functions has a smooth shape with distinct peak at the natural frequencies of the system. Therefore, it is more practical to use a displacement-based objective function (i.e., the sum of the mean-square interstory drift of the shear building) for this critical excitation problem.

In order to solve the problem, the constraints should be firstly selected. According to Eq. (9), the objective function at the time t_i is obtained as the product of $\bar{S}_w$ and the area of $H(t_i, \omega)$ in the specific interval $\tilde{\Omega}$. This means that the value of the objective function is proportional to $\bar{S}_w$. Considering the concepts of $\bar{S}_w$ and$\bar{s}_w$, there is no straightforward way to recommend an appropriate value of these parameters. Consequently, it is difficult to estimate what value of $\bar{s}_w$ is sufficient to make the final non-stationary input critical. Nevertheless, at least a reasonable assumption can be made for the ratio of $\bar{S}_w/\bar{s}_w$. Therefore, the method may be used to locate the rectangular function. However, for the applicability of the method, a new constraint should be considered, as proposed in the next section.

3. Upper bound of input energy as the new constraint

Generally, all critical excitation problems involve one (or more) constraint(s). These constraints are essential to make sure that the presented model of excitation is physically realistic and acceptable. However, the response of the problem significantly depends on the selection of these constraints. An inappropriate choice may lead to unrealistic or underestimated results. Therefore, it is essential to consider a constraint that captures the actual situation.

By setting constraints on the acceleration and velocity time-histories of the ground motion, Takewaki (2004) determined an upper bound of total input energy per unit mass of a record for a damped linear elastic system. This bound is well-defined by two curves that perfectly bound the actual input energy curve in the range of short and long periods (see Fig. 2). In Fig. 2, the first curve, which is entitled as “the credible bound for acceleration constraint” is obtained by setting a constraint on the time integral of squared ground acceleration. This curve provides an overview of the possible total energy. This energy is then limited by the second curve, which is determined based on setting a similar constraint on the velocity of the ground motion, in the range of long periods. This shows that the factors that cause changes in the velocity structures may lead to the generation of long period ground motions. The intersection point of these two curves may be considered as the possible dominant period. However, the maximum actual input energy does not necessarily concentrate at this period.

It is remarkable that in the Takewaki’s work (2004), the total input energy has been considered as the objective function of the problem to determine its upper bound for any given earthquake time-history. On the contrary, it can be effectively adopted as the constraint of the problem, to find critical excitations with a certain upper bound of total input energy. This will introduce a rational base to the problem to ensure a realistic model of the excitation.

The investigations of present paper on the time-histories of various ground motions indicate that even for an identical level of energy bound for acceleration constraint, indicated by black dashed-line in Fig. 2, the maximum amount of actual energy is not the same. Moreover, this maximum value may occur in different periods. Fig. 3 represents the total input energy of two different records of the 1979 Imperial Valley earthquake at the stations on the 19 and 27 kilometers far from the epicenter. As may be observed from Fig. 3, increase in distance is not led to a significant change in energy bound for acceleration constraint, but the bound of energy derived from the velocity constraint is substantially changed. By moving to the right, the energy content of record is increased in the range of long periods, while the maximum of actual energy is approximately doubled. In other words, despite having almost identical upper limit for acceleration constraint, maximum amount of actual energy is changed for the both value and position parameters, resulting a long period ground motion. Such a situation can be observed in other earthquakes. Fig. 4 represents the total input energy for two

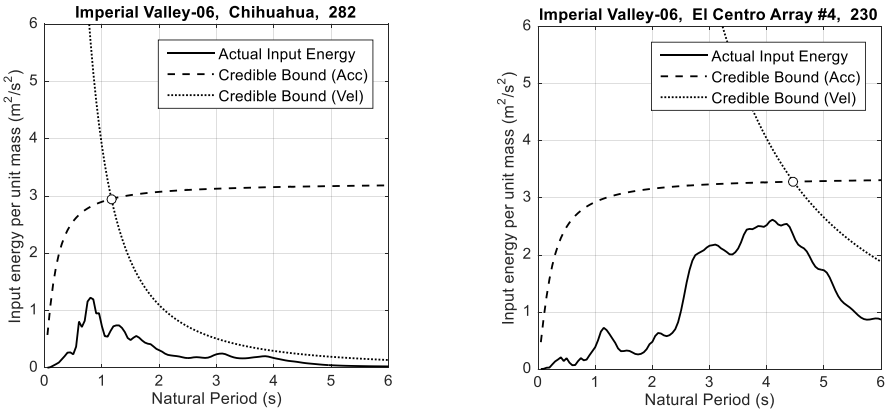

Fig. 3 Total input energy of two different records of the 1979 Imperial Valley earthquake

different records of Northridge, Chi-Chi and Loma Prieta earthquakes.

These examples clearly demonstrate that by a certain upper bound of the total input energy for acceleration constraint, various energy contents at different period ranges are feasible. This property let us to use this bound as an index to estimate the allowable range of input energy in similar ground motions. For example, consider a narrow-band record of the 1989 Loma Prieta earthquake (M=6.93) at Palo Alto station, located on a site with soil type D. Fig. 5 represents the total input energy of this ground motion (black line) as well as its credible bounds. From the upper bound of the total input energy of this record, it can be concluded that this earthquake may generate a ground motion with a maximum total input energy per unit mass up to 3 m^2/s^2 around the period of 1.5 second. This prediction can be easily confirmed since a real ground motion with the same site condition has been actually recorded during the same earthquake (dotted line). However, for other similar cases, the issue still remains. By considering an earthquake as a non-stationary random process, it may be concluded that existing ground motions are just a few realization of the corresponding event. Therefore, it is not so much safe to just rely on existing data. Let's consider a situation that the second ground motion of Fig. 5 (dotted line) has not been recorded. In such a case, it would be desirable to devise a method to find the worst realization of the same earthquake with a similar upper bound.

The upper bound of the input energy for acceleration constraint is completely defined by the following two parameters

$$\int |A(\omega)|^2 \, d\omega \qquad\qquad \max |A(\omega)|^2 \tag{10}$$

where $A(\omega)$ is the Fourier transform of the ground acceleration, $\ddot{u}_g(t)$. These two parameters may define a class of ground motions that existing record is just one realization of them. Therefore, it is reasonable to fix the upper bound of input energy, and let the excitation to change in amplitude and frequency content in such a way that the objective function is maximized. By this mean, and using a sample ground motion, a synthetic accelerogram may be generated with the same upper bound but different energy content.

Using Parseval's theorem the integral of Eq. (10) can be written as

$$I_A = \frac{\pi}{2g} \int a(t)^2 \, dt \tag{11}$$

where g denotes the gravity acceleration, and I_A indicates the well-known Arias Intensity parameter as written below

$$I_A = \frac{\pi}{2g} \int a(t)^2 \, dt \tag{12}$$

Therefore, in order to achieve a certain upper bound of the total input energy for acceleration constraint, the following constraints need to be satisfied

$$I_A \le \overline{I_A} \qquad\qquad \sup |A(\omega)| \le \overline{A} \tag{13}$$

where $\bar{I}_A$ and $\bar{A}$ are predefined input parameters which can be easily selected based on the corresponding values of a target ground motion. Moreover, in the case of Arias Intensity, a more robust determination can be adopted using probabilistic seismic hazard analysis methods (see for example: Travasarou *et al*. 2003). By this mean, any consideration on the earthquake hazard level can be incorporated into the method, as indicated by some seismic design codes.

When the first constraint is available, the second one can be determined using an empirical relationship that relates the maximum Fourier amplitude to the Arias Intensity. Fig. 6 illustrates a sample example of such relationships, where the data used were obtained from the PEER NGA database, including 449 earthquakes with three major fault mechanisms and a hypocentral distance ranging from 5 to 247 km. In addition, the database mostly covers soil types C and D (based on ASCE 7-10 Classifications). Since this critical excitation method needs all possible realizations of earthquakes, no further classifications are applied, and just one linear regression model is used to estimate the equation from the whole data.

If the interval of $\tilde{\Omega}$, at which the rectangular PSD function has a constant value, is assumed to remain unchanged after multiplying the random process $w(t)$ by the envelope function $c(t)$, an approximation of this interval can be given as follows

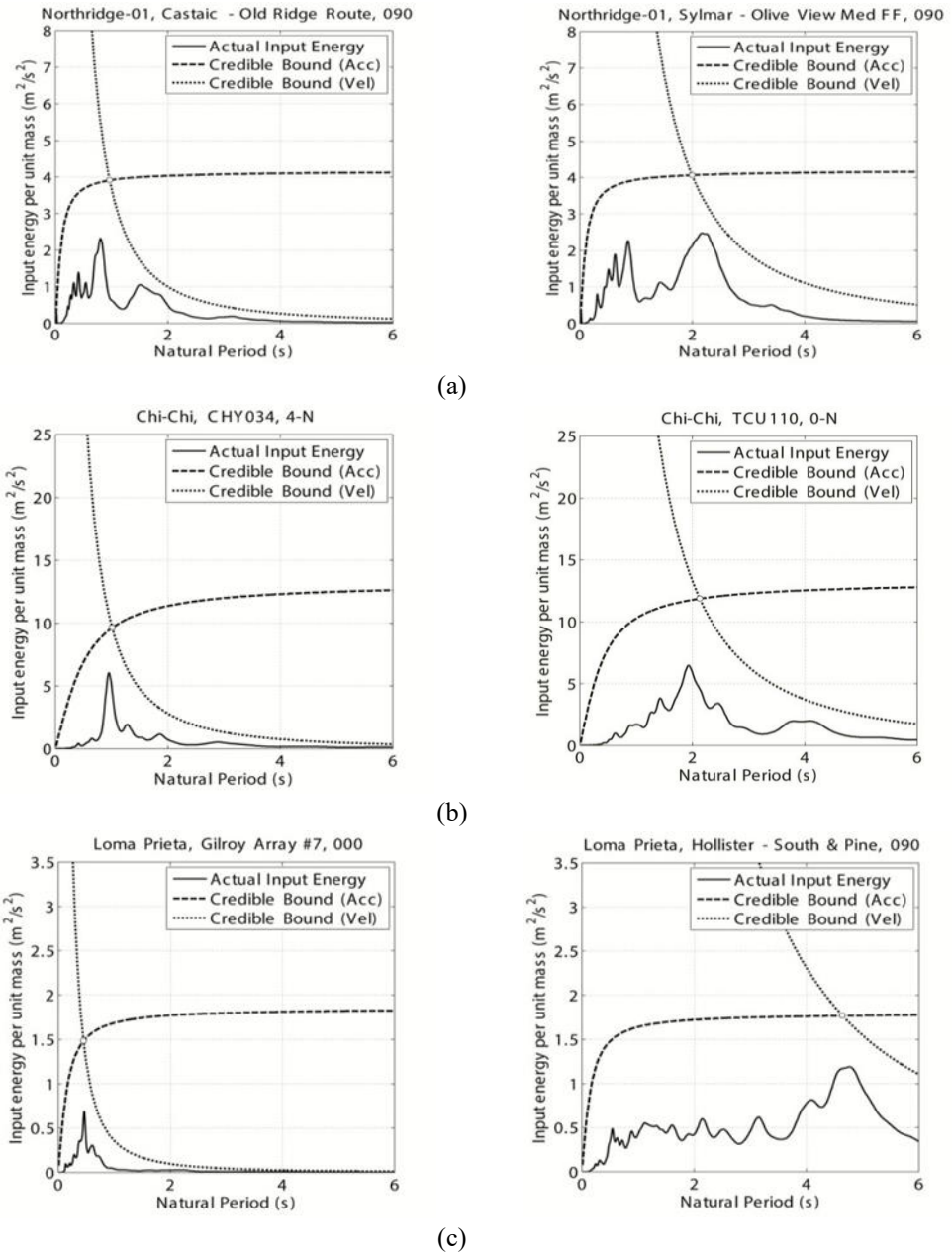

Fig. 4 Examples of total input energy for different records of (a) Northridge, (b) Chi-Chi, (c) Loma Prieta earthquakes with same upper bound of energy for acceleration constraint

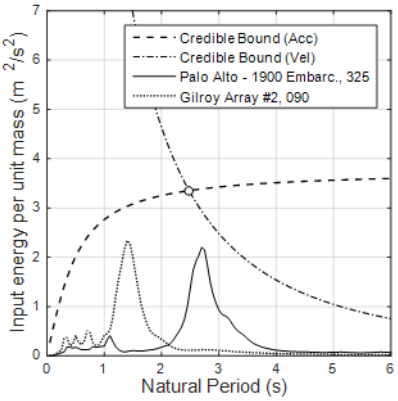

Fig. 5 Total input energy of the 1989 Loma Prieta earthquake at Palo Alto and Gilroy station

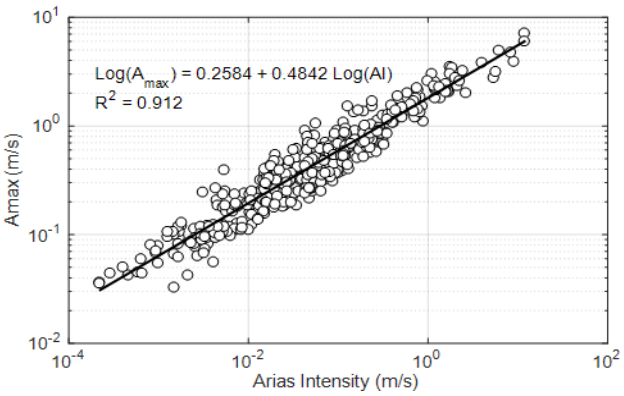

Fig. 6 A sample empirical relationship that relates the maximum Fourier amplitude to the Arias Intensity, based on data of the PEER NGA database

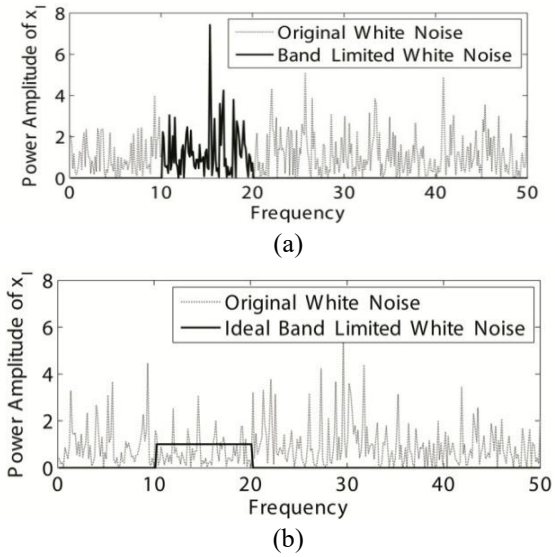

Fig. 7 Comparison of the PSD function of (a) original and (b) modified band limited white noises

$$\tilde{\Omega} = \frac{4g\overline{I_A}}{\overline{A}^2} \tag{14}$$

be employed here to find the rectangular PSD function.

To impose the constraints of Eq. (13), it is necessary to fix the peak of the Fourier transform, *A(ω)*, of the ground acceleration $\ddot{u}_g(t)$ as well as its Arias Intensity to pre-specified values. As illustrated earlier, $\ddot{u}_g(t)$ is defined as the product of an envelope function and a stationary Gaussian random process (see Eq. (1)). Due to the random nature of the problem, an iterative process is required to obtain the desired excitation with a certain Arias Intensity. To produce the non-stationary excitation, a band-limited stationary random process is required. However, as may be seen in Fig. 7(a), the Fourier Amplitude of such process is completely non-uniform with a wide range of variations. As the Arias Intensity of $\ddot{u}_g(t)$ is directly related to the area of its PSD function as indicated by Eq. (11), such variations can make it very difficult to satisfy the first condition. To resolve this problem, after generating the white noise, the corresponding Fourier amplitudes are modified to achieve a rectangular shape as depicted in Fig. 7(b). This adjustment helps to reach the solution with considerably less iterations as it preserves the area of the PSD function.

In order to calculate objective function, the maximum of the rectangular PSD function (i.e., $\bar{s}_w$), should be known (see Eq. (9)). In the conventional method, $\bar{s}_w$ is an input parameter of the problem. Conversely, by using new constraint, there is no way to determine $\bar{s}_w$ from the specified input parameter $\bar{A}$, since it is the maximum of the Fourier Amplitude of the final nonstationary random process $\ddot{u}_g(t)$, rather than the initial stationary random process $w(t)$. Nevertheless, an initial estimation of the objective function can be obtained from Eq. (9), using an assumption for $\bar{s}_w$, while the final excitation can be simply scaled so that the maximum value of its Fourier Amplitude is equal to the specified $\bar{A}$. As a consequence, the objective function is changed by this modification. However, it can be easily corrected by multiplying the corresponding scale factor to the initial estimation.

4. Numerical examples

4.1 Critical excitation procedure

In this section, the proposed method is used to determine critical excitation of three typical shear buildings of 10, 16 and 22 stories. These structures are selected as representative structures to cover the typical range of low-rise to high-rise buildings. These buildings are designed as steel moment frames, and the mass and stiffness of stories are then determined to establish the corresponding MDOF models. In other words, these models are well characterized by mass and stiffness of the stories, as illustrated in Table A of the Appendix. The natural vibration periods of the models are calculated as 0.96, 1.66 and 2.26 seconds, for shear buildings of 10, 16 and 22 stories, respectively. To find the critical excitation for the three models, a target ground motion can be used to define the constraints. This ground motion can be the largest event recorded near the site of the structure. As an example, the 1990 Manjil earthquake is selected as the target record, with constraint parameters of $\bar{I}_A$=1.86 (m/s) and $\bar{A}$=6.61 (m/s). Fig. 8 shows the upper bounds and the total input energy of the target ground motion. It can be seen that this record does not have remarkable energy content at the natural frequency of three models. Therefore, it is more reasonable to use corresponding critical excitations, which maximize the objective function with the same upper bound of energy.
The interval of $\tilde{\Omega}$ is determined using Eq. (14) as fallows

$$\tilde{\Omega} = \frac{4g\overline{I_A}}{\overline{A}^2} = \frac{4\times 9.81\times 1.86}{(6.61)^2} = 1.67\,(Rad/s) \tag{15}$$

The envelope function used herein is an exponential function which is defined as

$$c = e^{-\alpha t} - e^{-\beta t} \tag{16}$$

in which parameters α=0.10 and β=*0.35* are chosen so that a peak around 8 seconds and a duration of 50 seconds is achieved for the final critical excitations.

Fig. 9(a) shows the initial estimation of the objective functions for the three models obtained using Eq. (9) with the following assumption

$$\overline{s}_w \approx \overline{A}^2 \tag{17}$$

These estimations should be corrected using corresponding scale factors after generation of the final excitations (see Fig. 9(b)). Unlike the original method, the values of the objective functions are not of interest here, and only the critical rectangular PSD functions corresponding to the peak of these curves are important. Therefore, such modification to the objective function doesn't affect the solution of the problem.

Critical PSD functions of three models are shown in Fig. 10, from which it is observed that in 22-storey model, the rectangular function is determined as separate functions due

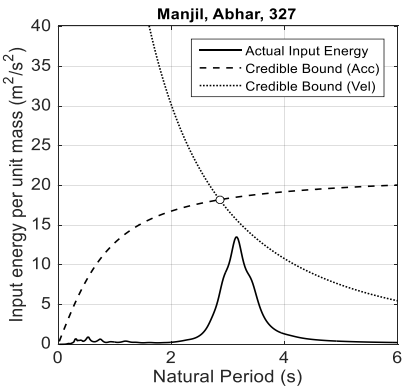

Fig. 8 Total input energy of the target record

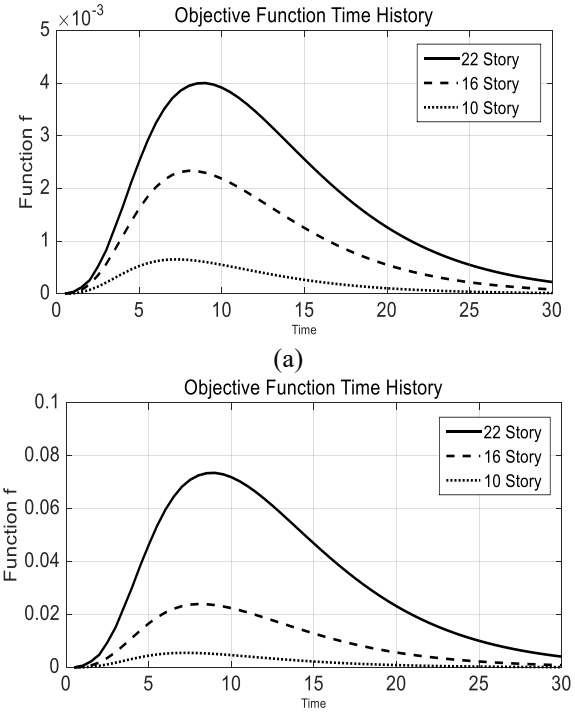

Fig. 9 (a) The initial and (b) corrected time-histories of the objective functions for the three models

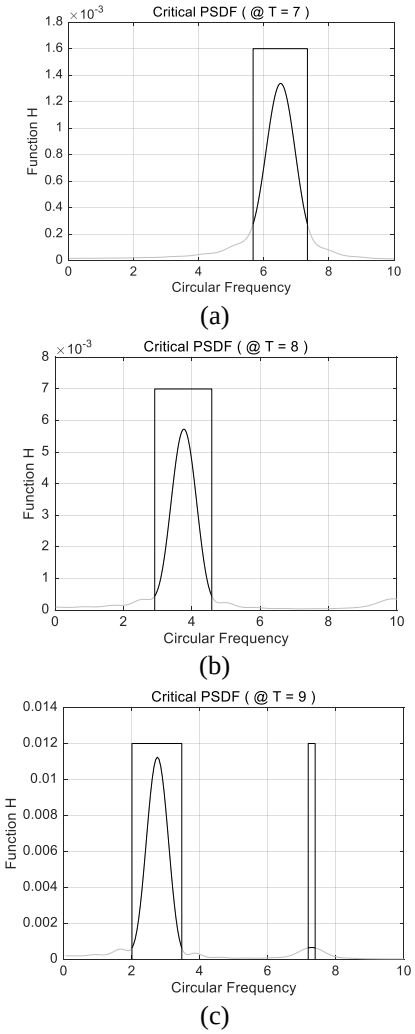

Fig. 10 Critical PSD functions (PSDFs) corresponding to the peak of objective functions of (a) 10-story, (b)16-story, and (c) 22-story shear buildings

to the significant effects of higher modes. It should be noted that the height of the rectangular PSD functions in these figures are represented schematically. Three sample time-histories of critical excitations generated based on these PSD functions are depicted in Fig. 11. The total input energy of these accelerograms as well as the target record is drawn in Fig. 12. As illustrated in this figure, the energy content of critical excitation for each model has been concentrated around its fundamental period. This ensures that these excitations will impose a more intense response to the structures compared with the target record. Moreover, preserving the upper bound of input energy to those of the target record provides a rational basis to avoid unrealistic and/or too-critical responses.

Additionally, it can be observed that the critical excitation of the 22-storey model, has another peak around the period of second mode of the model (1 second). This represents another advantage of this critical excitation method. Since the formulation of problem is based on the modal representation of structures, it is possible to exclude some modes from the calculation to accelerate the procedure (or, just to emphasis on the response of a certain mode).

4.2 Dynamic analyses

In order to investigate the reliability of overall dynamic response of a structure, when is subjected to the critical excitation, compared with a real ground motion, numerical dynamic analyses are carried out using three models of the previous section. For each model, an energy compatible target ground motion has been selected so that its maximum input energy is concentrated around the fundamental period of that model. To determine these target records, a database containing a large number of records has been considered, for which the maximum of input energy and corresponding period have been calculated. By plotting these parameters together, desired records can be readily determined. Therefore, these target ground motions can be considered as

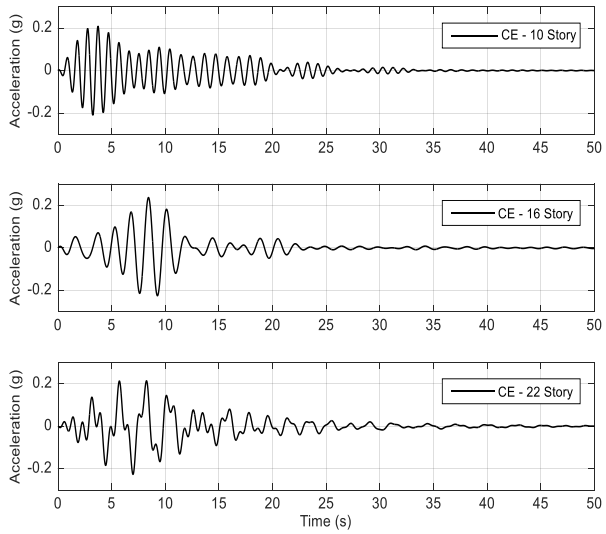

Fig. 11 Time-histories of generated critical excitations for the three models

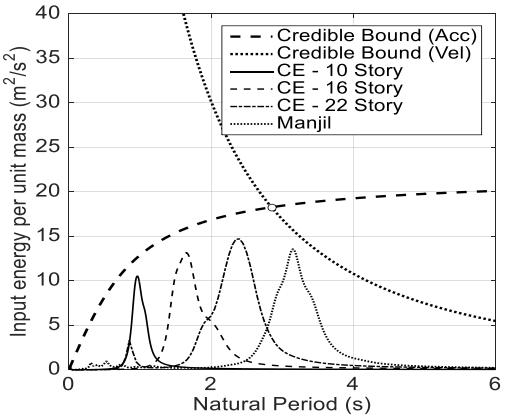

Fig. 12 Total input energies of critical excitations of three models

"real critical excitation" of each model. These ground motions will be used as benchmarks for verification of the generated critical excitations. Using these ground motions as well as the generated critical excitations, linear dynamic analyses are conducted, and the key parameters of response (i.e., maximum displacement, drift and acceleration of stories) are then compared.

Based on the target ground motions, the critical PSD functions of each model is determined using the method of the previous section, and three synthetic accelerograms are then generated for the three models. The total input energy of target ground motions of each model as well as those of the critical excitations are depicted in Fig. 13. This figure shows that there is a good conformity in overall shape of input energy between target records and the generated critical excitations. Figs. 14 to 16 represent the maximum story displacement, drift and acceleration of target records and corresponding critical excitations. Obviously, the pattern of maximum response of stories are similar in all cases. However, the responses due to the critical excitations are slightly larger as their maximum total input energy at the first mode of structures are larger.

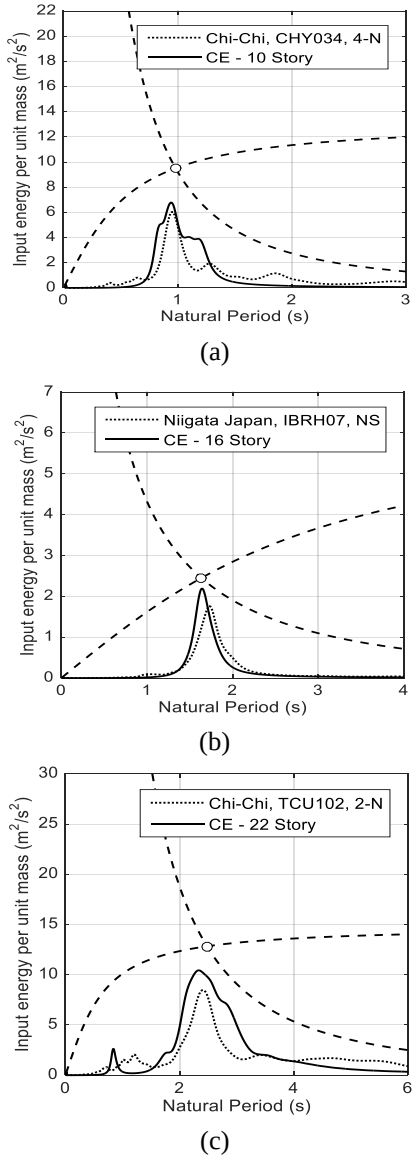

Fig. 13 The total input energy of target ground motions and critical excitations of (a) 10-story, (b), 16-story, and (c) 22-story models

4.3 Envelop function

The envelop function parameters (α and β) are important inputs of the problem and should be suitably defined in the present method. In order to investigate the effect of these parameters on the results of the problem, critical PSDF of -story model is determined using various parameters for the envelop function. To consider a wide range of inputs, two sets of envelope functions are considered: (1) for a constant α=0.1, while β decreases from 0.6 to 0.15, and then (2) for a constant β=0.6, while α increases up to 0.55. Since the variations are not so remarkable, only four cases of each set are represented here. Properties of these envelop functions for both sets are listed in Table 1. Given the selected duration for the envelop function (50 seconds), the lower limit for α is about 0.1, since for the values below 0.1, the envelop function does not reach zero at the end (see Fig. 17). The maximum value for α is equal to the β value, for

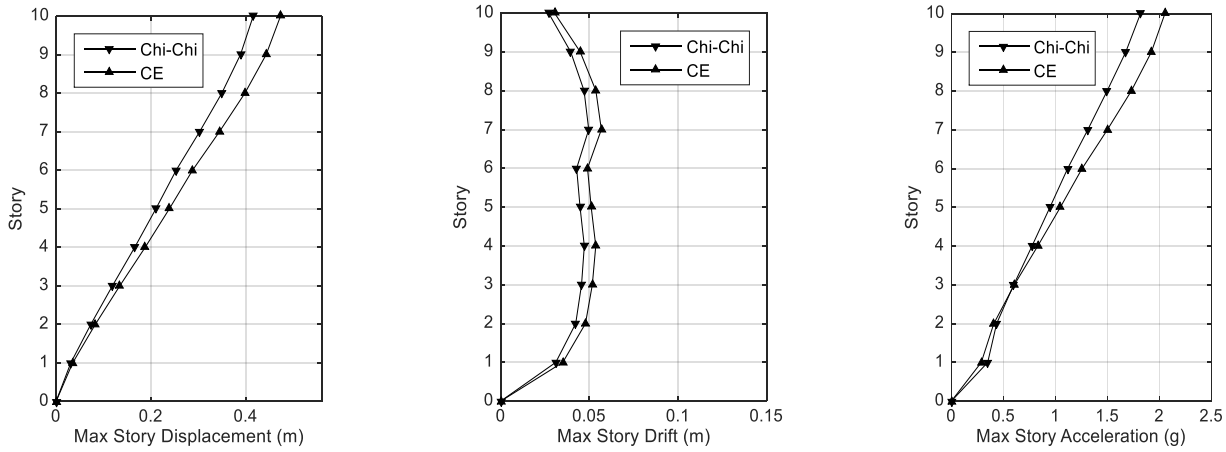

(a) (b) (c)

Fig. 14 (a) Maximum displacement, (b) maximum interstory drift, and (c) maximum absolute acceleration of 10-story model

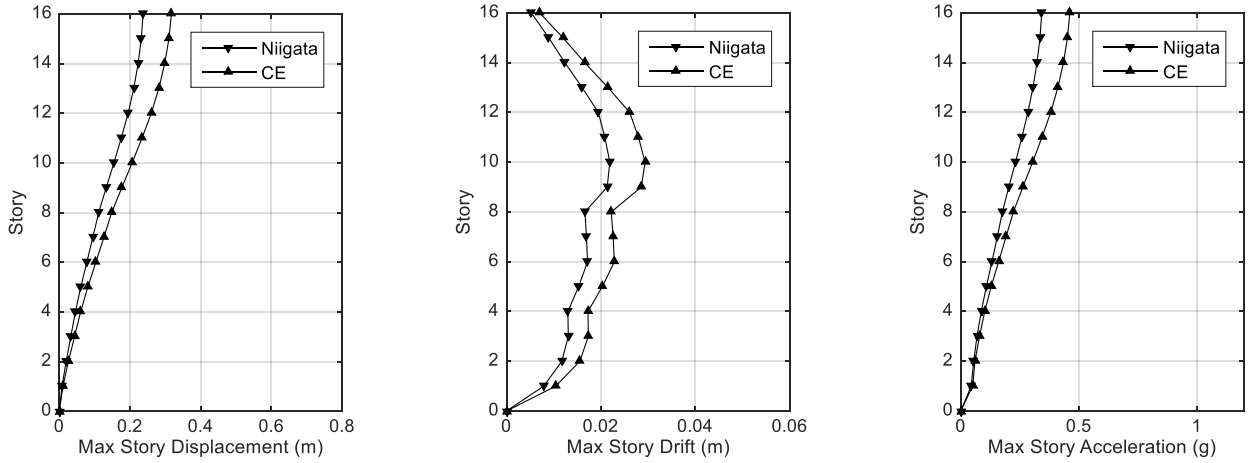

(a) (b) (c)

Fig. 15 (a) Maximum displacement, (b) maximum interstory drift, and (c) maximum absolute acceleration of 16-story model

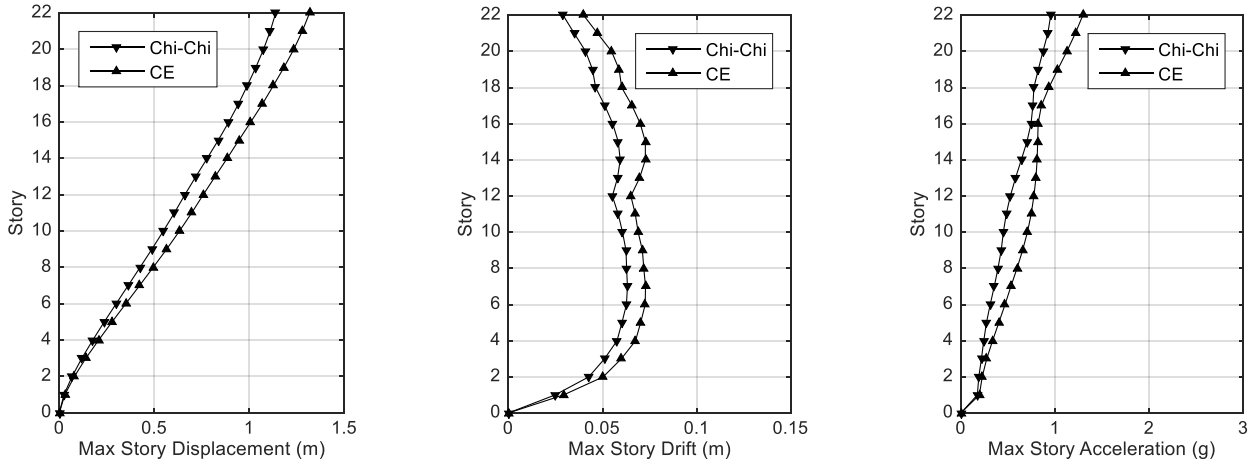

(a) (b) (c)

Fig. 16 (a) Maximum displacement, (b) maximum interstory drift, and (c) maximum absolute acceleration of 22-story model

which the envelope function will be equal to zero. Similarly, the minimum value for β would be equal to α.

The upper limit for β is chosen only to summarize the results. The time histories of considered envelop functions are illustrated in Fig. 18.

Fig. 19 shows the critical PSD functions for different envelop functions. It can be observed from this figure, although for each envelop function $H(t,w)$, and consequently

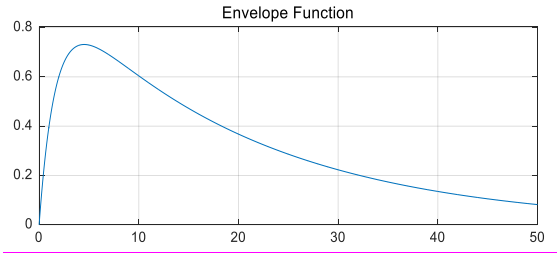

Fig. 17 The time history of considered envelop function (α=0.05 and β=0.6)

Table 1 Properties of envelop functions of both sets (1) and (2)

Function	α	β	Function	α	β
env 1	0.10	0.60	env 1	0.10	0.60
env 2	0.10	0.45	env 2	0.25	0.60
env 3	0.10	0.30	env 3	0.40	0.60
env 4	0.10	0.15	env 4	0.55	0.60

the initial estimation of the objective functions are different, the critical PSD functions are identical for all cases. Therefore, it may be concluded that the critical PSD functions are not sensitive to the parameters of this envelop function. As a result, these parameters can be arbitrarily selected to achieve a certain excitation with desired duration and peak position, which corresponds to those of the target record.

5. Conclusions

In this paper, a new critical excitation method for MDOF systems was developed. For the simplicity, a displacement-based objective function (The sum of the mean-square interstory drift of the shear building) has been used in this paper. Results of the present study may be summarized as follows:

- The main issue of using the critical excitation methods is the selection of appropriate constraints. It has been shown that the upper bound of earthquake input energy per unit mass called as "the credible bound for acceleration constraint" can be considered as a suitable constraint for the present critical excitation problem. This constraint provides a rational basis to prevent unrealistic and/or too-critical responses.
- The simple rectangular PSD function used in this paper can be effectively adopted to reproduce ground motions with narrow frequency content. The comparison of results of linear dynamic analysis of three MDOF models of shear buildings under critical excitations and target ground motions shows that the generated excitations can reasonably estimate the behavior of structures, including the maximum displacement, drift and absolute acceleration of stories.
- The critical PSD function of this problem is not sensitive to the parameters of the envelope function. In other words, changing the envelope function only changes the initial estimation of the objective function, which is corrected in the proposed procedure. As a result, parameters of the envelope function can be arbitrarily selected to achieve a certain excitation with desired duration and peak position, which corresponds to those of the target record.

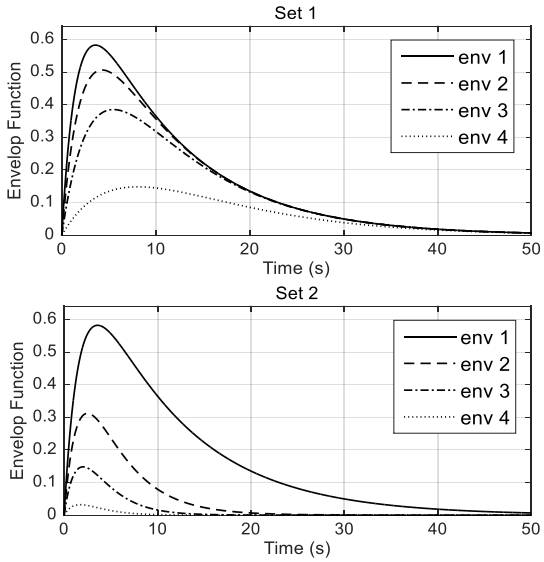

Fig. 18 The time histories of considered envelop functions of (a) set 1, and (b) set 2

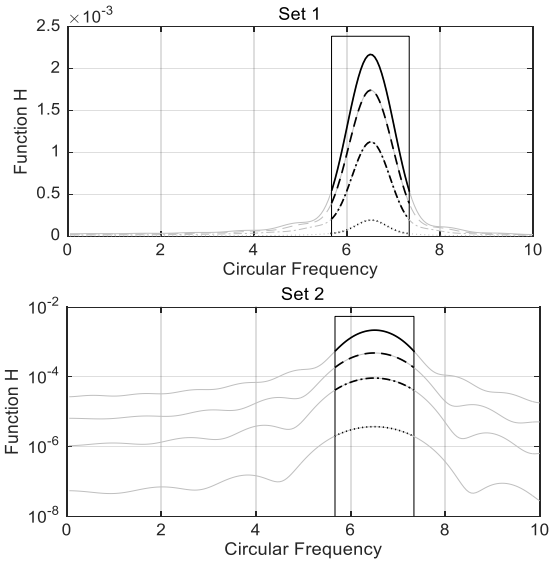

Fig. 19 Critical PSD functions for different envelop functions of (a) set 1, and (b) set 2

As the rectangular PSD function does not provide any control over the peak frequency of the excitation, the method is more efficient for narrow-band target records. However, the present method may be extended using a non-rectangular or continues PSD function in order to resolve this issue, which is currently being followed by the authors.

References

Abbas, A.M. and Manohar, C.S. (2007), "Reliability-based vector nonstationary random critical earthquake excitations for

parametrically excited systems", *Struct. Saf.*, **29**(1), 32-48. https://doi.org/10.1016/j.strusafe.2005.11.003.

Ahmadi, G. (1979), "On the application of the critical excitation method to aseismic design", *J. Struct. Mech.*, **7**(1), 55-63. https://doi.org/10.1080/03601217908905312.

Akehashi, H. and Takewaki, I., (2019), "Optimal viscous damper placement for elastic-plastic MDOF structures under critical double impulse", *Front. Built Environ.*, **5**(20). http://hdl.handle.net/2433/237499.

Ashtari, P. and Ghasemi, S.H. (2013), "Seismic design of structures using a modified non-stationary critical excitation", *Earthq. Struct.*, **4**(4), 383-396. http://dx.doi.org/10.12989/eas.2013.4.4.383.

Au, S.K. (2006), "Critical excitation of SDOF elastoplastic systems", *J. Sound Vib.*, **296**(4-5), 714-733. https://doi.org/10.1016/j.jsv.2006.01.034.

Cetin, H., Aydin, E. and Ozturk, B., (2019), "Optimal design and distribution of viscous dampers for shear building structures under seismic excitations", *Front. Built Environ.*, **5**, 1-13. https://doi.org/10.3389/fbuil.2019.00090.

Drenick, R.F. (1970), "Model-free design of aseismic structures", *J. Eng. Mech.*, **96**(4), 483-493.

Fukumoto, Y. and Takewaki, I. (2015), "Critical earthquake input energy to connected building structures using impulse input", *Earthq. Struct.*, **9**(6), 1133-1152. http://hdl.handle.net/2433/241753.

Ghasemi, S.H. and Ashtari, P. (2014), "Combinatorial continuous non-stationary critical excitation in MDOF structures using multi-peak envelope functions", *Earthq. Struct.*, **7**(6), 895-908. http://dx.doi.org/10.12989/eas.2014.7.6.895.

Iyengar, R.N. (1972), "Worst inputs and a bound on the highest peak statistics of a class of non-linear systems", *J. Sound Vib.*, **25**(1), 29-37.

Khatibinia, M., Gholami, H. and Kamgar, R. (2018), "Optimal design of tuned mass dampers subjected to continuous stationary critical excitation", *Int. J. Dyn. Cont.*, **6**(3), 1094-1104. https://doi.org/10.1007/s40435-017-0386-7.

Kamgar, R., Samea, P. and Khatibinia, M. (2018), "Optimizing parameters of tuned mass damper subjected to critical earthquake", *Struct. Des. Tall Spec. Build.*, **27**(7), e1460. https://doi.org/10.1002/tal.1460.

Kamgar, R. and Rahgozar, R. (2015), "Determination of critical excitation in seismic analysis of structures", *Earthq. Struct.*, **9**(4), 875-891. http://dx.doi.org/10.12989/eas.2015.9.4.875.

Kamgar, R., Shojaee, S. and Rahgozar, R. (2015), "Rehabilitation of tall buildings by active control system subjected to critical seismic excitation", *Asian J. Civ. Eng.*, **16**(6), 819-833.

Kojima, K., Saotome, Y. and Takewaki, I. (2018), "Critical earthquake response of a SDOF elastic-perfectly plastic model with viscous damping under double impulse as a substitute for near-fault ground motion", *JPN Arch. Rev.*, **1**(2), 207-220. https://doi.org/10.1002/2475-8876.10019.

Lekshmy, P.R. and Raghukanth, S.T.G. (2015), "Maximum possible ground motion for linear structures", *J. Earthq. Eng.*, **19**(6), 938-955. https://doi.org/10.1080/13632469.2015.1023472.

Moustafa, A. (2009), "Critical earthquake load inputs for multi-degree-of-freedom inelastic structures", *J. Sound Vib.*, **325**(3), 532-544. https://doi.org/10.1016/j.jsv.2009.03.022.

Moustafa, A. (2011), "Damage-based design earthquake loads for single-degree-of freedom inelastic structures", *J. Struct. Eng.*, **173**(3), 456-467. https://doi.org/10.1061/(ASCE)ST.1943-541X.0000074.

Nigdeli, S.M. and Bekdas, G. (2017), "Optimum tuned mass damper design in frequency domain for structures", *KSCE J. Civ. Eng.*, **21**(3), 912-922. https://doi.org/10.1007/s12205-016-0829-2.

Srinivasan, M., Ellingwood, B. and Corotis, R. (1991), "Critical base excitations of structural systems", *J. Eng. Mech.*, **117**(6), 1403-1422. https://doi.org/10.1061/(ASCE)0733-9399(1991)117:6(1403).

Takewaki, I. (2001a), "A new method for non-stationary random critical excitation", *Earthq. Eng. Struct. Dyn.*, **30**(4), 519-535. https://doi.org/10.1002/eqe.21.

Takewaki, I. (2001b), "Nonstationary random critical excitation for acceleration response", *J. Eng. Mech.*, **127**(6), 544-556. https://doi.org/10.1061/(ASCE)0733-9399(2001)127:6(544).

Takewaki, I. (2002), "Critical excitation for elastic–plastic structures via statistical equivalent linearization", *Prob. Eng. Mech.*, **17**(1), 73-84. https://doi.org/10.1016/S0266-8920(01)00030-3.

Takewaki, I. (2004), "Bound of earthquake input energy", *J. Struct. Eng.*, **130**(9), 1289-1297. https://doi.org/10.1061/(ASCE)0733-9445(2004)130:9(1289).

Takewaki, I. (2006), "Probabilistic critical excitation method for earthquake energy input rate", *J. Eng. Mech.*, **132**(9), 990-1000. https://doi.org/10.1061/(ASCE)0733-9399(2006)132:9(990).

Tamura, G., Kojima, K. and Takewaki, I., (2019), "Critical response of elastic-plastic SDOF systems with nonlinear viscous damping under simulated earthquake ground motions", *Heliyon*, **5**(2), e01221. https://doi.org/10.1016/j.heliyon.2019.e01221.

Travasarou, T., Bray, J.D. and Abrahamson, N.A., (2003), "Empirical attenuation relationship for Arias intensity", *Earthq. Eng. Struct. Dyn.*, **32**(7), 1133-1155. https://doi.org/10.1002/eqe.270.

Zhai, C.H. and Xie, L.L. (2007), "A new approach of selecting real input ground motions for seismic design: The most unfavourable real seismic design ground motions", *Earthq. Eng. Struct. Dyn.*, **36**(8), 1009-1027. https://doi.org/10.1002/eqe.669.

CC

Appendix

In the current critical excitation method, the structural models are considered as shear buildings. So the model is completely characterized by its mass and stiffness. The mass and stiffness of all stories for the three models are shown in Table A.

Table A Mass and stiffness of stories for the three models used in section 4

Story No.	22 Story		16 Story		10 Story	
	Mass*	Stiffness**	Mass	Stiffness	Mass	Stiffness
1	414860	1701350	412830	1471800	430410	1277980
2	414860	984909	412830	988388	430410	928388
3	414860	826031	412830	864713	430410	844713
4	414860	727993	412830	857139	430410	757486
5	413290	683171	406830	709315	408320	712393
6	413290	645994	406830	600467	408320	678391
7	412040	620681	406830	588987	397870	481029
8	412040	606758	406830	565453	397870	406600
9	412040	588528	401170	407792	387820	335683
10	412040	571246	401170	362881	387820	255646
11	410470	569132	388910	335355		
12	410470	564321	388910	319770		
13	405690	502010	388910	308930		
14	405690	451029	388910	296260		
15	405690	424393	383260	285646		
16	405690	405066	383260	246260		
17	405690	385741				
18	405690	365055				
19	405690	319683				
20	405690	274456				
21	391560	225790				
22	391560	175709				

* Mass unit: kg
** Stiffness unit: kN/m